

Mitigating baryon feedback bias in cosmic shear through a theoretical error covariance in the matter power spectrum

Alessandro Maraio^{*}, Alex Hall, Andy Taylor

Institute for Astronomy, University of Edinburgh, Royal Observatory, Blackford Hill, Edinburgh EH9 3HJ, UK

Last updated 16 October 2024

ABSTRACT

Forthcoming cosmic shear surveys will make precise measurements of the matter density field down to very small scales, scales which are dominated by baryon feedback. The modelling of baryon feedback is crucial to ensure unbiased cosmological parameter constraints; the most efficient approach is to use analytic models, but these are limited by how well they can capture the physics of baryon feedback. We investigate the fitting and residual errors of various baryon feedback models to a suite of hydrodynamic simulations, and propagate these to cosmological parameter constraints for cosmic shear. We present an alternative formalism to binary scale-cuts through the use of a theoretical error covariance, which is a well-motivated alternative using errors in the power spectrum modelling itself. We depart from previous works by modelling baryonic feedback errors directly in the matter power spectrum, which is the natural basis to do so and thus preserves information in the lensing kernels. When including angular multipoles up to $\ell_{\max} = 5000$, and assuming *Euclid*-like survey properties, we find that even multi-parameter models of baryon feedback can introduce significant levels of bias. In contrast, our theoretical error reduces the bias in Ω_m and S_8 to acceptable levels, with only a modest increase in parameter variances. The theoretical error approach bypasses the need to directly determine the per-bin ℓ_{\max} values, as it naturally suppresses the biasing small-scale information. We also present a detailed study of how flexible HMCODE-2020, a widely-used non-linear and baryonic feedback model, is at fitting a range of hydrodynamical simulations.

Key words: gravitational lensing: weak — large-scale structure of Universe — methods: statistical

1 INTRODUCTION

Cosmic shear is the coherent distortion in the apparent shapes of galaxies due to the matter distribution of the large-scale structure of the universe (Bartelmann & Schneider 2001; Bartelmann 2010; Kilbinger 2015). These distortions are sensitive to the total matter inhomogeneities along the line-of-sight, and thus are a powerful probe of the non-luminous dark matter, which ordinarily cannot be directly observed using telescopes. Cosmic shear is also sensitive to the detailed physics of baryons, particularly on small scales, within the Universe. By making accurate measurements, along with robust theoretical modelling, cosmic shear is able to provide detailed knowledge about the physics and geometry of the universe.

Cosmic shear surveys have already placed tight constraints on the fundamental physics and properties of our universe, especially on the growth of structure parameter S_8 , defined as $S_8 \equiv \sigma_8 \sqrt{\Omega_m/0.3}$. The results from existing surveys have been well-studied, with data coming from the Kilo-Degree Survey (KiDS-1000) (Heymans et al. 2021; Asgari et al. 2021; Li et al. 2023b), the Dark Energy Survey (DES-Y3) (Abbott et al. 2022; Amon et al. 2022; Secco et al. 2022; Doux et al. 2022), and Hyper Suprime-Cam (HSC-Y3) (Li et al. 2023a; Dalal et al. 2023).

Over the next decade, an unprecedented amount of high-quality cosmic shear data will be released. This will come from the recently

launched *Euclid* space telescope (Laureijs et al. 2011; Mellier et al. 2024), the Legacy Survey of Space and Time (LSST) at the *Rubin* observatory (Abate et al. 2012), and the *Roman* space telescope (Spergel et al. 2015). Since the quality and quantity of cosmic shear data that is expected to be produced is so vast, the accuracy of the theoretical modelling is required to be as equally precise.

While the majority of the matter in the universe is dark matter, which only interacts gravitationally, the baryons in the universe, while appearing to be lighter in total mass, have an equally large affect on the dynamics of the universe – particularly on small scales. Baryons are responsible for the heating and cooling of gas, the creation and demise of stars, and play an important part in the feedback from Active Galactic Nuclei (AGN), which can have considerable impact on the matter power spectrum over a wide range of scales (van Daalen et al. 2011).

The modelling of baryon feedback and its effects on cosmic shear cosmology has been discussed extensively in the literature, with very many different methods and implementations proposed to mitigate its effects. These include Schneider & Teyssier (2015), Giri & Schneider (2021), Aricò et al. (2021), Huang et al. (2019), Salcido et al. (2023) and Mead et al. (2020), among many others. Cosmic shear is a measurement in angular-space due to the necessity of using coarse photometric redshift estimates, and so this makes the measurements of cosmic shear sensitive to high- k wavenumbers throughout any ℓ values in the angular power spectrum. It is at high k where feedback effects become relevant.

^{*} Contact e-mail: marai@roe.ac.uk

A popular approach to mitigating baryonic effects in cosmic shear analyses is to introduce scale-cuts into the data-vector. Here, physically smaller scale elements in the data vector beyond a cut-off, either in real-space θ_{\min} or in Fourier-space ℓ_{\max} , are completely discarded even if high signal-to-noise observations have been taken. These scale-cuts are often dependent on the redshift of the source galaxies, as for further away redshift bins the same physical scale is given by larger θ or smaller ℓ . One issue that arises with such scale-cuts is that it by definition is a *hard cut* on the data. For example, if it was chosen that $\ell_{\max} = 2000$, then $\ell = 2000$ would be included in an analysis whereas the $\ell = 2001$ mode would be excluded, even though these modes will be highly coupled and have very similar theoretical uncertainties. The use of these binary scale cuts have been discussed heavily in previous cosmic shear results, most recently in the Dark Energy Survey's Year 3 results (real-space) (Krause et al. 2021; Abbott et al. 2022), the Kilo-Degree Survey fourth data release (KiDS-1000, in real-space) (Li et al. 2023b), and Hyper Suprime-Cam's Year 3 results (harmonic-space) (Dalal et al. 2023).

Since the use and location of a hard scale cut could be considered somewhat unphysical, in the sense that we have two consecutive data points one with little error and one with infinite error, we investigate and present results for an alternative: the use of a theoretical error covariance which acts as a soft scale cut that is informed by our inability to correctly model baryonic feedback down to arbitrarily small scales. This has been explored in the literature previously, with the theory being originally presented in Baldauf et al. (2016), expanded upon in Sprenger et al. (2019), and applied to mock cosmic shear analyses in Moreira et al. (2021), among others (Pellejero-Ibanez et al. 2023). Baryonic feedback effects directly impact the matter power spectrum, which is then integrated over to produce effects in the lensing angular power spectrum. Thus, when we model our theoretical uncertainties coming from baryonic feedback, it is most natural to do so in the matter power spectrum and propagate these uncertainties to the angular power spectrum. Moreira et al. (2021) investigated theoretical uncertainties with respect to the *angular* power spectrum, and so we are revisiting this formalism but extending it to the underlying matter power spectrum. Since baryonic feedback contaminates only the matter power spectrum, not the lensing kernels associated with cosmic shear, isolating the errors associated with the matter power spectrum then propagating these to the angular power spectrum is a sensible alternative approach. The theoretical uncertainties approach is similar to analytic marginalisation of small-scale physics, which also results in an additional term to the covariance matrix (Kitting & Taylor 2011).

This paper is structured as follows: in Section 2 we outline the need for analytic baryon feedback models and the use of hydrodynamical simulations, Section 3 discusses our methodology for constructing our theoretical error covariance, in Section 4 we present our results for cosmological parameter constraints using a selection of baryon feedback models, and Section 5 summarises our findings.

2 MODELLING BARYONIC FEEDBACK IN THE MATTER POWER SPECTRUM

Accurate evaluations of the non-linear dark-matter-only matter power spectrum is of extreme importance to any cosmic shear analysis (Schneider et al. 2016). There are numerous ways to accurately evaluate this. For example, many models descend from the original halo model presented in the early 2000s (Seljak 2000; Peacock & Smith 2000; Cooray & Sheth 2002; Smith et al. 2003): the HALOFIT model presented in Takahashi et al. (2012), and HMCODE models that

originate with HMCODE-2015 (Mead et al. 2015), then HMCODE-2016 (Mead et al. 2016), and most recently HMCODE-2020 (Mead et al. 2020). All these models serve to provide accurate predictions for the non-linear dark-matter-only matter power spectrum as a function of cosmological parameters.

The most accurate way of modelling baryonic feedback physics is through full hydrodynamical cosmological simulations (hydro-sims) (van Daalen et al. 2011; Vogelsberger et al. 2020). There are many different hydro-sims within the literature, which mainly differ in their implementations of sub-grid physics. There are suggestions that these sub-grid physics differences are connected to the gas fraction in galaxy groups and clusters (Salcido & McCarthy 2024). These simulations are extremely computationally expensive due to the need for large volumes, to reduce cosmic variance and capture clustering on cosmological scales, and the need to model small-scale behaviour, which directly impacts the larger-scale clustering. Thus, these simulations need sufficient resolution else the baryonic feedback physics which we wish to capture will simply be washed out on larger scales and also sufficient volume. This presents a challenging dynamic range problem, hence the very many different simulations that implement these range of physics.

To isolate the effect of baryonic physics on the matter power spectrum when compared to the dark-matter-only non-linear power spectrum, we use the baryon response function, $R(k, z)$, defined as

$$R(k, z) \equiv \frac{P^{\text{Hy}}(k, z)}{P^{\text{DM}}(k, z)}, \quad (1)$$

which isolates the effects of baryon physics from the general non-linear spectrum, and is especially useful for reducing the effects of cosmic variance on the power spectrum when using hydro-simulations. This ratio is approximately insensitive to the cosmological parameters that $P^{\text{Hy}}(k)$ and $P^{\text{DM}}(k)$ were generated using, provided that they are the same cosmology (van Daalen et al. 2020; Elbers et al. 2024). This makes the baryon response function especially useful when trying to compare predictions between different hydro-sims run at different cosmologies. Since every hydro-sim has a different implementation of their astrophysical processes, the range of curves for $R(k, z)$ can be extremely broad. Figure 1 plots this ratio for a verity of different hydro-sims for three redshifts. This shows the general behaviour of $R(k, z)$ that has been well explored previously (van Daalen et al. 2011): there is a dip in expected power on non-linear scales ($1 \text{ hMpc}^{-1} \lesssim k \lesssim 10 \text{ hMpc}^{-1}$ at $z = 0$) due to baryon feedback processes, such as AGN, jets, and supernovae, expelling matter reducing clustering, while the dramatic increase on highly non-linear scales ($k \gtrsim 10 \text{ hMpc}^{-1}$) is due to additional clustering from the ability of baryons to undergo radiative cooling, increasing small-scale clustering, and from star formation within the simulations (Chisari et al. 2019). Also shown in Figure 1 is the level of scatter in the prediction of $R(k, z)$ for different hydro-sims, with the depth and location of the suppression and location of the upturn highly simulation dependant with very little common consensus between these simulations. van Daalen et al. (2020) has shown that much of this scatter in the predictions for the suppression in the simulations can be explained by how the amplitude of the suppression is strongly correlated with the mean baryon fraction in haloes of mass $\sim 10^{14} M_{\odot}$ (Salcido & McCarthy 2024).

Due to the large scatter in the predictions of the hydro-sims, we take an agnostic approach to their results: we assume that each of these simulations are equally trustworthy, and thus any of these predictions for their $R(k, z)$ must be equally reliable. We must also assume that the true description of our Universe lies somewhere in this ensemble in order to correctly match observational data. Hence,

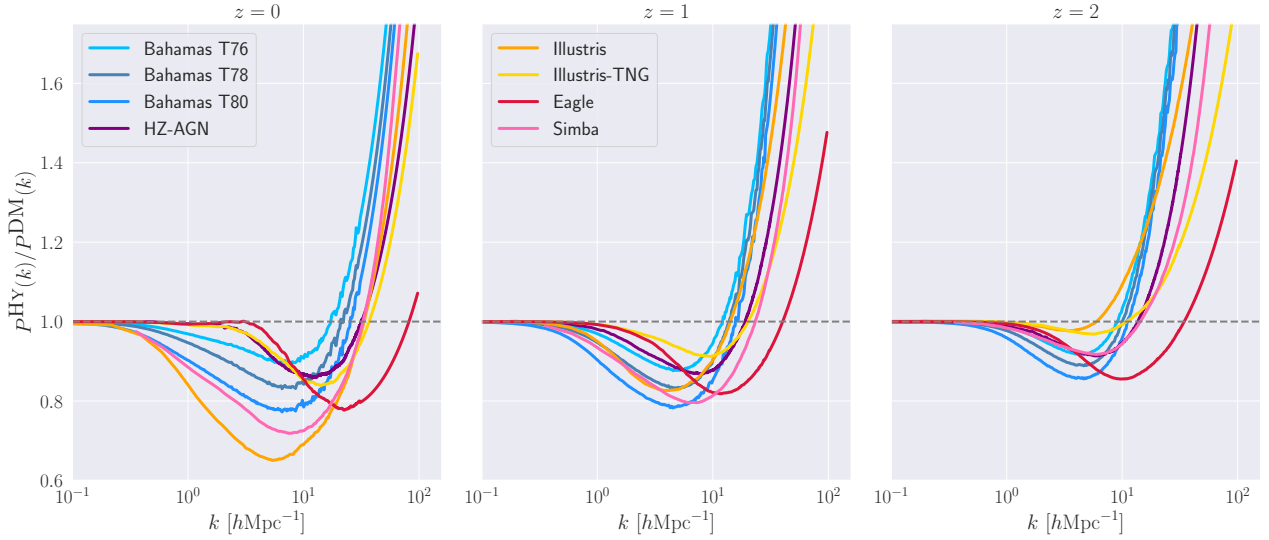


Figure 1. Ratios of the matter power spectrum with baryonic feedback in to their dark-matter-only counterparts at redshifts 0, 1, and 2, for various hydrodynamical simulations, as given in Table 1. Here, ‘BAHAMAS TXY’ corresponds to the same underlying BAHAMAS hydro-sim, just run at different ΔT_{heat} values, which corresponds to the amplitude of AGN feedback within their simulation (McCarthy et al. 2017). Note that SIMBA was run on a smaller box-size with respect to the other simulations (as shown in Table 1), and thus we do not have access to data below a certain k for SIMBA, which is much larger than the smallest k modes available for the other hydro-sims.

any baryon physics model must be able to recreate all of these curves in order for us to sufficiently trust that it could potentially capture the real physics of our Universe. This level of scatter in the hydro-sims has lead to the development of many baryonic physics models, especially those which aim to match the simulations through neural-network emulator methods, such as the BACCO emulator presented in Aricò et al. (2021). BACCO claims accuracy 1-2% for scales $1 \text{ hMpc}^{-1} < k < 5 \text{ hMpc}^{-1}$ and redshifts $0 < z < 1.5$, and again finds that the most important parameter that controls baryon feedback physics is the gas fraction per halo mass. Furthermore, BCEMU (Giri & Schneider 2021) implements the ‘baryonification model’ prescription (Schneider et al. 2019) which claims percent-level accuracy for scales below $k \sim 10 \text{ hMpc}^{-1}$ at redshifts $z < 2$.

We are motivated to find correct descriptions of baryon feedback physics due to their large impact on results obtained from cosmic shear surveys. Future Stage-IV cosmic shear surveys hope to probe extremely small scales, up to a maximum multipole of $\ell_{\text{max}} \sim 5000$ (Laureijs et al. 2011). These small angular scales probe the highly non-linear regime in the matter power spectrum, as shown in Figure 2. Here, we plot the cumulative sum of the derivate of the angular power spectrum coefficients C_ℓ at certain ℓ values as a function of k . This shows the relative contribution for each k mode to each C_ℓ value. Hence, we find that if we hope to probe angular scales up to $\ell = 5000$, then we need to have a strong understanding of the matter power spectrum up to scales $k \sim 10 \text{ hMpc}^{-1}$ – including the details of baryonic physics. If these scales are not correctly modelled, then this could induce catastrophic biases in a cosmic shear analysis (Semboloni et al. 2011; Huang et al. 2019), particularly for the constraints on dark energy (Copeland et al. 2018). The alternative is to reduce the maximum multipole ℓ_{max} in our analyses, though this discards potentially useful cosmological information.

This motivates us to test the accuracy of baryonic feedback models up to these small scales, and assess how different treatments of baryonic physics impact constraints obtained from forthcoming cosmic shear surveys.

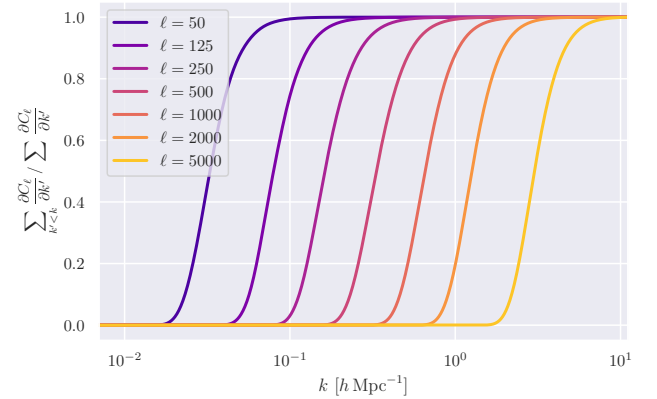


Figure 2. Cumulative sum of the derivate of the cosmic shear power angular power spectrum coefficients C_ℓ , at certain ℓ modes, with respect to the wavenumber k in the Limber integral (Equation 4). The sum of the derivatives for each multipole is normalised to unity for easy comparison between different modes. This includes the contributions from the lensing kernels and the matter power spectrum. Derivatives were taken for a Gaussian source redshift distribution located at $\bar{z} = 0.33$ and width $\sigma_z = 0.15$.

2.1 Theoretical error formalism

Since we do not have models of baryonic physics that completely match our complete set of hydrodynamical simulations, there will always be some residual error for any given model of baryon feedback physics as a function of scale and redshift. Rather than treating our models as a perfectly known quantity and limiting our scales of interest, we can directly incorporate these known errors through the use of the ‘theoretical uncertainty’ formalism first presented in Baldauf et al. (2016). We now have a theoretical error data-vector \mathbf{e} , which quantifies the difference between the true, underlying physical model and what our approximative methods calculate, which is

bound by an envelope E . This theoretical error has its associated covariance matrix, \mathbf{C}^E , which can be written as a function of the amplitude of the error, E , and a correlation matrix ρ as

$$\mathbf{C}^E = E \rho E. \quad (2)$$

In the Gaussian approximation, we can simply model the inclusion of the theoretical error on the likelihood as simply the addition of our theoretical error covariance, \mathbf{C}^E , to our existing data covariance matrix (which includes the contributions from cosmic variance), \mathbf{C}^D , to give

$$\mathbf{C}^{\text{TOT}} = \mathbf{C}^D + \mathbf{C}^E. \quad (3)$$

The theoretical error formalism can be, in principle, applied to any effect that changes summary statistics that is not yet perfectly modelled. This approach of marginalising over the errors in the model was first applied to baryonic physics effects for cosmic shear surveys in [Moreira et al. \(2021\)](#), where they modelled the errors and correlations directly in ℓ -space. They constructed several versions of the error envelope function $E(\ell)$, all featuring the similar term of the error ratio of best-fit C_ℓ values to the values generated from hydro-sims. They also assumed a Gaussian-like function in $(\ell - \ell')^2$ for their correlation matrix, with a characteristic correlation length L determining the widths of the correlation matrix.

Since baryonic effects directly change the matter power spectrum, which is then propagated to cosmic shear summary statistics, we are motivated to investigate the theoretical errors in k -space for the matter power spectrum and then propagate those to ℓ -space. There is no theoretical error associated with the lensing kernels, so by isolating the theoretical uncertainties to the matter power spectrum only, we might hope to preserve information from geometry this way. The task now becomes one to find an appropriate theoretical error envelope function E and correlation matrix ρ in k -space.

3 METHODOLOGY

3.1 Modelling forthcoming cosmic shear surveys

We use the standard prescription for the cosmic shear power spectrum ([Bartelmann & Schneider 2001](#); [Bartelmann 2010](#); [Kilbinger 2015](#)) where the power spectrum is, for tomographic redshift bins labelled by a and b , is given as

$$C_\ell^{ab} = \frac{9}{4} \frac{\Omega_m^2 H_0^4}{c^4} \int_0^{\chi_{\text{max}}} d\chi \frac{g_a(\chi) g_b(\chi)}{a^2(\chi)} P\left(k = \frac{\ell}{\chi}, z = z(\chi)\right), \quad (4)$$

where $a(\chi)$ is the scale factor, P is the non-linear matter power spectrum, and $g(\chi)$ is the lensing kernel given as

$$g_a(\chi) = \int_\chi^{\chi_h} d\chi' n_a(\chi') \frac{f_K(\chi' - \chi)}{f_K(\chi')}, \quad (5)$$

where $n(\chi)$ is the probability density of source galaxies as a function of comoving distance. To evaluate the non-linear matter power spectrum with baryonic feedback, we used HMCODE-2020 with $T_{\text{AGN}} = 7.8$.

Since every galaxy has an intrinsic ellipticity, this introduces a shape noise term into the power spectrum with a flat value N_ℓ given as

$$N_\ell^{ab} = \frac{\sigma_\epsilon^2}{\bar{n}} \delta^{ab}, \quad (6)$$

where σ_ϵ is the standard deviation of the intrinsic galaxy ellipticity dispersion per component, \bar{n} is the expected number of observed

galaxies per steradian, and δ^{ab} is the Kronecker- δ symbol. We assume *Euclid*-like values where it is expected that 30 galaxies per square arcminute will be observed, but we divide these into five photometric redshift bins, giving $\bar{n} = 6$ gals/arcmin² ([Laureijs et al. 2011](#)). We take $\sigma_\epsilon = 0.21$.

We use five Gaussian redshift bins with means located at $\bar{z} = \{0.33, 0.66, 1.0, 1.33, 1.66\}$ all with standard deviation of $\sigma_z = 0.15$. This gives us 15 unique power spectrum combinations and 120 unique covariance matrix blocks.

We model the Gaussian covariance matrix as the four-point function ([Blanchard et al. 2020](#)), given by

$$\text{Cov}[C_\ell^{ab}, C_{\ell'}^{cd}] = \frac{C_\ell^{ac} C_\ell^{bd} + C_\ell^{ad} C_\ell^{bc}}{(2\ell + 1) f_{\text{sky}}} \delta_{\ell\ell'}, \quad (7)$$

where f_{sky} is the fraction of sky observed by the cosmic shear survey. We take a *Euclid*-like value of $f_{\text{sky}} = 0.35$.

To reduce the dimensionality of our power spectrum and covariance matrices, we bin the power spectrum. We use linear binning of five bins up to $\ell = 100$, and then use logarithmic binning with twenty bins from $\ell = 100$ to $\ell = 5000$. We use an ℓ -mode weight of $\ell(\ell + 1)$ when binning.

3.2 Constructing our k -space theoretical covariance

As outlined in Section 2.1, the theoretical error formalism requires us to quantify an error envelope function E and a correlation matrix ρ , and since our uncertainties from baryonic physics are best specified in k -space, we will first construct our k -space covariance matrix. We will first discuss the construction of our envelope function E .

There is no absolute choice for the functional form of E . [Moreira et al. \(2021\)](#) investigated many choices for the form of E , with the ‘mirror’ envelope being a good fit to the data. Here, we follow their method and take the maximum deviation for each k -mode and redshift across a suite of hydrodynamical simulations to the best-fitting values of a baryon feedback model (see Section 3.6). This gives the maximum relative difference in the baryonic response function (Equation 1) as

$$\Delta R(k, z) = \max_{k, z} \left| \frac{R^{\text{HYDRO}}(k, z)}{R^{\text{MODEL}}(k, z)} - 1 \right|. \quad (8)$$

We then turn this into an amplitude by multiplying by a fiducial dark-matter-only power spectrum,

$$E(k, z) = P^{\text{DM}}(k, z) \Delta R(k, z). \quad (9)$$

where $P^{\text{DM}}(k, z)$ was evaluated using the HMCODE-2020 DM-only model.

With our amplitude function specified, we now wish to construct our k -space correlation matrix. Here, we are considering the correlations between two pairs of points (k_1, z_1) and (k_2, z_2) . We follow previous works that have employed the theoretical uncertainties approach (for example [Baldauf et al. \(2016\)](#); [Sprenger et al. \(2019\)](#); [Chudaykin & Ivanov \(2019\)](#); [Moreira et al. \(2021\)](#)) by choosing a factorisable Gaussian correlation matrix of the form

$$\rho[(k_1, z_1), (k_2, z_2)] = \exp \left[-\frac{\log(k_1/k_2)^2}{\sigma_{\log k}^2} \right] \exp \left[-\frac{(z_1 - z_2)^2}{\sigma_z^2} \right], \quad (10)$$

where $\sigma_{\log k}$ and σ_z are the characteristic correlation scales in $\log k$ - and redshift-space, respectively. In our fiducial analyses, we used

values of $\sigma_{\log k} = 0.25$ and $\sigma_z = 0.25$. These values were motivated from Figure 1 where we see that the baryonic response function $R(k, z)$ is correlated on scales of approximately a quarter of a decade in $\log k$ space with approximately the same coupling in redshift-space. We discuss the effects of changing $\sigma_{\log k}$ and σ_z in Section 4.4.5.

We are motivated to use factorisable Gaussians since we know that baryon feedback has a relatively local effect on the matter power spectrum, that is neighbouring wavenumbers and redshifts behave similarly and thus should have highly correlated covariances, whereas vastly different wavenumbers and redshifts have very different evolutionary physics, and thus should be less correlated. Furthermore, we are motivated to use the logarithmic differences in k -space since our wavenumbers span many orders of magnitude (see Figure 1), and thus an ordinary difference might not properly reflect this.

Combining our envelope function and correlation matrix, we find that our complete k - and redshift-space covariance matrix is given by

$$\text{Cov}[(k_1, z_1), (k_2, z_2)] = P^{\text{DM}}(k_1, z_1) \Delta R(k_1, z_1) P^{\text{DM}}(k_2, z_2) \Delta R(k_2, z_2) \times \exp\left[-\frac{\log(k_1/k_2)^2}{\sigma_{\log k}^2}\right] \times \exp\left[-\frac{(z_1 - z_2)^2}{\sigma_z^2}\right]. \quad (11)$$

We note that by working directly with errors in the matter power spectrum, which is the underlying quantity that we have limited knowledge in modelling (not the angular power spectrum values), this should capture the full phenomenology of the errors in baryonic feedback effects on the matter power spectrum. This contrasts with the work of [Moreira et al. \(2021\)](#) which also aims to mitigate baryonic physics effects through the use of a theoretical uncertainty, though they quantify their theoretical uncertainty through the differences in the angular power spectrum values.

3.3 Propagating covariances to ℓ -space

With our k - and redshift-space covariance matrix specified, we can now propagate this into an ℓ -space covariance matrix, which can then be added to the data covariance to give our overall covariance matrix.

Equation 4 gave the cosmic shear power spectrum as the Limber integral of the matter power spectrum weighted by the geometrical factors. Hence, if we now want to propagate our uncertainties in the $P(k)$ into an additional covariance matrix for the C_ℓ values, we can integrate this again, which yields

$$\text{Cov}[C_{\ell_1}^{ab}, C_{\ell_2}^{cd}] = \left[\frac{9}{4} \frac{\Omega_m^2 H_0^4}{c^4} \right]^2 \times \int_0^{\chi_{\max}} \int_0^{\chi_{\max}} d\chi_1 d\chi_2 \frac{g_a(\chi_1) g_b(\chi_1)}{a^2(\chi_1)} \frac{g_c(\chi_2) g_d(\chi_2)}{a^2(\chi_2)} \text{Cov}[(k_1, z_1), (k_2, z_2)], \quad (12)$$

where $k_1 = \frac{\ell_1}{\chi_1}$ and $k_2 = \frac{\ell_2}{\chi_2}$. We are motivated to use Limber's approximation here to simplify the double integral since the low ℓ region in which the approximation is imprecise will have a negligible contribution to the total covariance.

3.4 Numerical evaluation of the matter power spectrum with baryon feedback

Our construction of the (k, z) -space covariance matrix can be applied to any model of baryon feedback, with models ranging from purely

analytical methods using the Zel'dovich approximation ([Mohammed & Seljak 2014](#)), to semi-analytic models (e.g. HMCODE, [Mead et al. 2020](#)), to purely numerical emulation (e.g. BACCO, [Aricò et al. 2021](#) and BCCMU, [Schneider et al. 2019](#)).

We have chosen HMCODE-2020 as our model of choice for the matter power spectrum and baryonic feedback response since they claim that their dark-matter-only spectrum has RMS errors of less than 5 per-cent, and that their baryonic feedback response is accurate to within the 1 per-cent level for redshifts $z < 1$ and scales ($k < 20 h\text{Mpc}^{-1}$), over a range of cosmologies ([Mead et al. 2020](#)). Thus, HMCODE-2020 is a natural choice for computing the matter power spectrum for use in cosmic shear analyses, which is confirmed by its use in recent major cosmic shear results such as the joint KiDS-1000–DES-Y3 analysis ([Abbott et al. 2023](#)).

HMCODE-2020 comes in two distinct flavours for modelling baryon physics:

- A full six-parameter description with free-parameters of the halo concentration, B , the stellar mass fraction in haloes, f_\star , and the halo mass break scale, M_b , along their redshift evolution counterparts. The redshift evolution for each physical parameter X is given by the fixed form of $X(z) = X_0 \times 10^{z \bar{X}_z}$.
- A one-parameter version where the feedback temperature T_{AGN} encapsulates the combined baryon physics of the full model. The one-parameter model was constructed by fitting a linear relationship to the six-parameter version using the BAHAMAS simulations. Since the one-parameter model was specifically constructed to the BAHAMAS simulations, there is no guarantee of its accuracy to other hydrodynamical simulators or even the baryon physics of our own Universe.
- We also test a three-parameter version, which is analogous to the six-parameter model but with fixed redshift evolution. This is a useful test as there arises significant degeneracies between the amplitude and redshift evolution of each parameter, and thus by fixing its evolution we can test if this extra degree of freedom is necessary.

While a more general description of baryon feedback physics should have more freedom to better match different physical models, it comes at the cost of additional nuisance parameters which needs to be included and marginalised over in any analysis. This could slow down the convergence of analysis pipelines, and in the case of very many parameter models, unnecessarily decreasing constraints on the core cosmological parameters due to the need to excessively marginalise over these baryonic nuisance parameters. Hence, while we are focusing on the inclusion of theoretical uncertainties into our analysis pipeline, we also look at how going from a one- to three- to six-parameter baryonic feedback model changes our results.

3.5 Chosen hydrodynamical simulations

We make use of the ‘power spectrum library’ presented in [van Daalen et al. \(2020\)](#)¹ and from the CAMELS Project ([Ni et al. 2023](#))² to build up a suite of six hydrodynamical simulations (with three flavours of the BAHAMAS simulations) as shown in Table 1. This gives us a wide range of baryon feedback models against which we can benchmark our analytic models to.

¹ <https://powerlib.strw.leidenuniv.nl>

² <https://camels.readthedocs.io/>

Table 1. The six hydrodynamical simulations used in this work to benchmark and compare models of baryon feedback physics to.

Hydro-sim	Box-size (Mpc)	Number of particles	Baryonic mass resolution [M_\odot]	Cosmology	Reference
Bahamas	400/ h	2×1024^3	$7.66 \times 10^8 h^{-1}$	WMAP 9	McCarthy et al. (2017)
Horizon-AGN	100/ h	1024^3	8.3×10^7	WMAP 7	Chisari et al. (2018)
Illustris	106.5	1820^3	1.6×10^6	WMAP 7	Nelson et al. (2015)
Illustris-TNG 100	75/ h	2×1820^3	$9.44 \times 10^5 h^{-1}$	Planck 2015	Springel et al. (2018)
Eagle	100	1504^3	1.81×10^6	Planck 2013	Schaye et al. (2015)
Simba	25/ h	1024^3	2.85×10^5	Planck 2013	Davé et al. (2019)

3.6 Fitting HMCode to hydrodynamical simulations

Armed with our three baryon feedback models and a suite of hydrodynamical simulations, we can now go about performing a best-fit analysis of our models to the hydro-sims in order to quantify each model’s maximum deviation as a function of wavenumber and redshift (Equation 8). To do so, we performed a maximum likelihood fit where we simultaneously fitted across redshifts $z \leq 2$ with flat weighting in redshifts, and wavenumbers over the range $0.01 h\text{Mpc}^{-1} \leq k \leq 20 h\text{Mpc}^{-1}$ with a k^2 weighting on each wavenumber to roughly approximate the cosmic variance contribution. We are free to choose an arbitrary k -mode weighting since our envelope function is arbitrary, and so there is no correct choice for either a k - or z -mode weight here. We experimented with flat, and a pure cosmic variance weight of k^3 , and settled on our k^2 weighting as somewhere in between. Note that, since we use equal spacing in $\log(k)$, we find $\Delta \log k = [\Delta k] / k$ when summing over k . This gives our loss function for each model and hydro-sim as

$$\mathcal{L} = \sum_{k,z} k^2 \left(R^{\text{HYDRO}}(k, z) - R^{\text{HMCODE}}(k, z) \right)^2. \quad (13)$$

The HMCode power spectra were generated at the same cosmology at which the hydro-sims were run at, with the minimisation routine just varying the astrophysical baryonic parameters. The Minuit optimiser, a robust optimiser as part of the CosmoSis³ analysis framework (Zuntz et al. 2015), was used to maximise the fit for the baryonic parameters. Since we there is freedom in the form of the weight function for each (k, z) -mode, different choices for the analytic form of \mathcal{L} effectively adds little to that freedom.

3.7 Fitting the C_ℓ values

To obtain estimates for the biases in cosmological parameters due to baryon feedback, many MCMC analyses were run. We used a custom CosmoSis pipeline using the PolyChord nested sampler (Handley et al. 2015a,b) with parameters `LivePoints = 1000`, `num_repeats = 60`, `boost_posteriors = 10`, and `tolerance = 0.001` for all analyses. We sampled only over Ω_c and A_s for our cosmological parameters, giving results in terms of Ω_m , σ_8 , and S_8 , since cosmic shear surveys are most sensitive to these cosmological parameters. Thus, any induced bias will be greatest in these parameters. In addition, we also sample over our one, three, and six baryonic feedback parameters, depending on the model, with wide priors, as shown in Table 2, on these nuisance parameters.

We ran analyses with just the ordinary Gaussian covariance matrix for our cosmic shear fields (Equation 7), and with the additional theoretical error covariances (Equation 12) added to the Gaussian covariance (Equation 3).

³ <https://cosmosis.readthedocs.io/>

Table 2. Uniform priors used for the HMCode baryonic feedback models. T_{AGN} is used only in the one-parameter models, with the three-parameter model sampling over just the individual amplitude parameters (X_0), and the six-parameter model including the redshift dependence too (X_z).

Parameter	Uniform prior
T_{AGN}	[4.0, 12.0]
B_0	[0.25, 7.0]
B_z	[-0.5, 0.5]
$f_{\star,0}$	[0.0, 5.0]
$f_{\star,z}$	[-5.0, 5.0]
$M_{b,0}$	[5.0, 20.0]
$M_{b,z}$	[-2.5, 2.5]

A Gaussian likelihood was used, which has been shown to be a good approximation to the full Wishart distribution on the cut-sky (Upham et al. 2021; Hall & Taylor 2022) under the assumption of Gaussian-only terms in the covariance matrix, which we are employing.

We generate the input cosmic shear C_ℓ values for each hydro-sim by taking each hydro-sim’s baryon response function R and multiplying it by HMCode’s dark-matter only matter power spectrum at the hydro-sim’s cosmology, giving

$$P^{\text{HY}}(k, z) = R(k, z) \times P^{\text{HMCODE-DM}}(k, z). \quad (14)$$

Thus, we are isolating the effects of baryon feedback in the C_ℓ values, and not studying other effects, for example the details of the non-linear matter power spectrum.

4 RESULTS

4.1 Results of fitting HMCode to hydro-sims

The first task was to fit our three HMCode baryon physics models to the suite of hydro-sims. Figure 3 shows the goodness of fit statistic for each hydro-sim for our 1-, 3-, and 6-parameter model. We see that the 1-parameter model generally provides a poor fit to our hydro-sims due to its inability to match the general baryon feedback models. When we extend the generality to 3- and 6-parameters, the goodness of fit increases which matches our intuition that a more general model with higher degrees of freedom should do a better job at matching arbitrary data sets. It should be noted that the HMCode 1-parameter model was specifically designed to closely match the BAHAMAS simulations, and so it is no surprise that it has a better fit to BAHAMAS than other simulations.

While our goodness of fit values provide a valuable insight into how well our three models fit the simulation data overall, we can look at the ratios for the HMCode predictions to the hydro-sims results to see how our fit changes with scales. Figure 4 plots the ratio of the best-fit HMCode model to the hydro-sims baryonic response function for

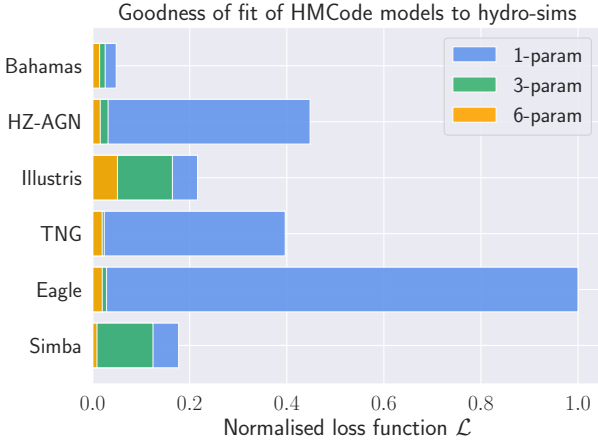


Figure 3. Goodness of fit statistics for the HMCode 1-, 3-, and 6-parameter models for our suite of hydro-simulations. We plot the reduced loss function \mathcal{L} values (Equation 13 divided by the total number of data-points across our redshift and wavenumber ranges) since each hydro-sim has a different number of redshift bins and wavenumbers that the power spectra were evaluated at, normalised to the one-parameter model for the Eagle hydro-sim. Here, we see the inflexibility of the 1-parameter model results in significant deviations across all simulations (except BAHAMAS which it was constructed to fit well), which indicates a poor fit to the data. Extending the model to 3- and then 6-parameters further increases the goodness of fit to simulations, since we open up additional degrees of freedom within the model. We note that the feedback within ILLUSTRIS is quite extreme, and thus produces a degraded fit even with the six-parameter model.

our three n -parameter models as a function of scale at redshift $z = 0$. We see that the more general three- and six-parameter models are better able to match the hydro-sims than the one-parameter model, which is to be expected from more general models, and is shown by a reduced amplitude in the relative differences. We also see the extreme nature of the ILLUSTRIS simulation, where the six-parameter model can only poorly match its feedback.

4.2 Constructing the envelope

Now that we know how well each of our feedback models match our suit of hydro-sims, we can combine these to form our ‘envelope function’ $\Delta R(k, z)$ introduced in Equation 8. ΔR encodes the maximum deviation of each baryon feedback model to all hydro-sims as a function of wavenumber and redshift. This acts as a standard deviation to our theoretical error as each baryon feedback model has an inherent uncertainty and we have quantified this with the envelope of the residual discrepancies between the hydro-sims and the best-fitting $R(k, z)$ for each simulation.

We plot $\Delta R(k, z)$ in Figure 5, which shows our envelope function as a function of wavenumber k for select redshift values. We see that, in general, the errors increase with k which corroborates our understanding that our theoretical models do worse the smaller scales we probe. We also see that higher redshifts tend to produce a better fit across all of the models which can be understood through Figure 1: we see that at higher redshifts, the suppression due to baryons is reduced, smoothing our response function R , and also moving the suppression to smaller wavenumbers. This acts to allow our baryonic feedback models to better match the hydro-sims, though our errors do increase to very large values on at high k at high redshifts.

We note that the six parameter model has a distinctive double-

hump feature, which is a direct result of the poor fit to ILLUSTRIS on scales $10^{-1} h\text{Mpc}^{-1} < k < 1 h\text{Mpc}^{-1}$, as shown in Figure 4. One could remove ILLUSTRIS when constructing the maximum deviation envelope, and such this double-hump would no longer appear.

4.3 Constructing the ℓ -space theoretical uncertainty covariance matrix

Our numerical envelope in (k, z) -space can then be doubly integrated (Equation 12) to give us our ℓ -space covariance matrix. Figure 6 plots the ratio of the block diagonals of the covariance matrix with our additional theoretical error to that without theoretical error. We see that for ℓ modes below $\ell \simeq 200$ there is no effect of our theoretical error covariance, since these ℓ modes are unaffected by baryon feedback physics. Above this, we see that our theoretical error covariance acts to increase the total covariance, thus suppressing ℓ modes here and down-weighting them in our likelihood analyses. We note that this is strongly dependent on the combination of spectra considered, with low redshift bins having a smaller error than those at high redshift (which is a direct consequence of our baryon feedback modelling being less accurate at high redshift). We see that, because we are considering the covariances of the auto-spectra only, that the ratios tend to unity at high- ℓ which is due to the inclusion of shape noise (which dominates the auto-spectra for large ℓ modes) in the overall covariance matrix.

We plot the total theoretical uncertainty matrix, \mathbf{C}^{E} in Figure 7. Here, we see that the amplitude of the full matrix reflects what is shown in the diagonals only of Figure 6, that the amplitude of the theoretical uncertainties generally grow as we consider further away redshift bin combinations (going from bottom-left to top-right). We also see that while each sub-block of the full matrix peaks along its diagonal, it has significant support with comparable values for many off-diagonal entries, which acts to boost the effects of the theoretical uncertainties over what the diagonal values can provide.

4.4 Parameter constraints and biases

Using our three different baryon feedback models, we can run our MCMC pipeline to estimate the biases in our cosmological parameters, the total matter density Ω_m and the lensing amplitude S_8 , with and without our additional theoretical error. We take each hydrodynamical simulations’ baryon feedback response function as the ground truth input values into our cosmic shear pipeline (Equation 14). We run our analyses for each baryon feedback model against each hydro-sim, with and without the additional theoretical error to determine the biases on the cosmological parameters due to the effects of baryon feedback.

4.4.1 Binary scale-cuts

We first look at the value of the biases in Ω_m and S_8 as a function of maximum multipole when using a traditional binary scale-cuts approach. Figure 8 plots the Ω_m , σ_8 , and S_8 offset contours for the Simba hydro-sim when analysed using the one-parameter model for a range of maximum ℓ -modes allowed in the analysis. We see that only the $\ell_{\text{max}} = 500$ analysis produces results that are consistent with the input parameters to within 1σ , with even the $\ell_{\text{max}} = 1000$ analysis producing biased results. Each subsequent analysis where we increase the maximum ℓ -mode serves to both increase the raw bias in the cosmological parameters (since the high ℓ -modes capture more of the impact from baryon feedback) and reduce the area of the

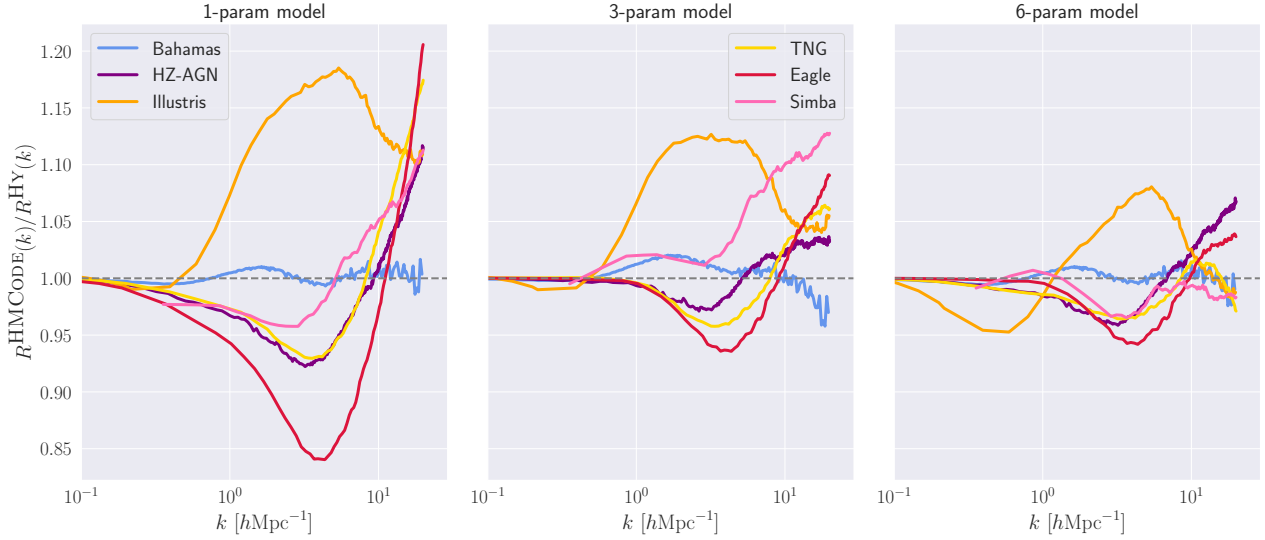


Figure 4. Ratios of the best-fitting HMCODE one-, three-, and six-parameter models to the underlying hydro-sims baryonic response function R at redshift $z = 0$. We see that HMCODE tends to fit the data better, as given by the smaller amplitude, as we increase the generality of the model, which is to be expected. Note that we fitted across all redshifts of each of the hydro-sims for $z \leq 2$, where here we are just plotting the $z = 0$ slice. Similar curves are found at higher redshifts.

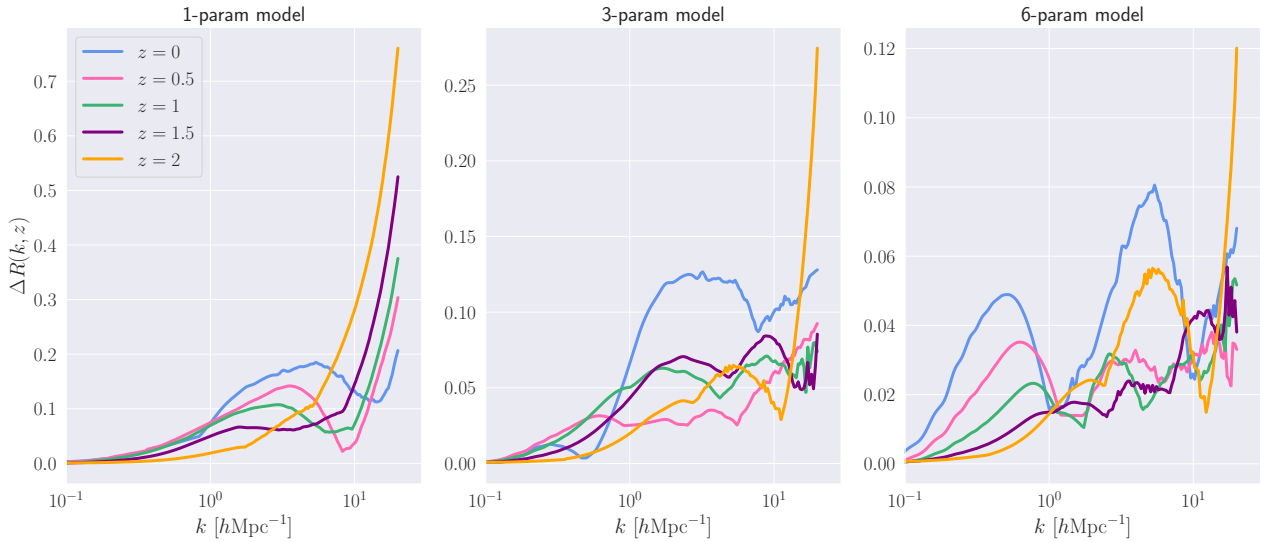


Figure 5. Our envelope function $\Delta R(k, z)$ encoding the maximum deviation of our three HMCODE models to the hydro-sims as a function of wavenumber k plotted for select redshifts. We see that the amplitude of our envelope decreases as we go from one- to three- to six-parameters (as noted by the decreasing values in each of the panel's individual y-axes), and so we assign less theoretical uncertainties to those models that better match the data. The apparent noisy behaviour of these curves is due to numerical noise in the hydro-sims, but also from our choice of envelope function, which uses the absolute value of the error ratio.

contours (since we are now including the more constraining higher ℓ -modes), which vastly increases the relative bias in the cosmological parameters.

Hence, if we were to introduce a binary scale-cut for our data that keeps the $\Delta\Omega_m - \Delta S_8$ to be consistent within 1σ , a cut slightly larger than $\ell_{\max} = 500$ might be made for our idealised Stage-IV like cosmic shear survey. However, to avoid making these analysis decisions ourselves, which have little physical motivation behind them and apply simultaneously to all hydro-sims in our ensemble, we can turn to our theoretical error modelling instead of making binary scale-cuts.

4.4.2 Including a theoretical error covariance

Tables 3 and 4 summarises our results for the biases in Ω_m and S_8 , respectively. Here, we present the amplitude of the bias, that is the difference in the mean of our MCMC chains to the fiducial value, and the relative bias, which is the difference divided by the reported standard deviation from the MCMC chains for each parameter, with and without the effects of our additional theoretical error. The baryonic feedback parameters for each model are marginalised over when we present results for Ω_m , σ_8 and S_8 .

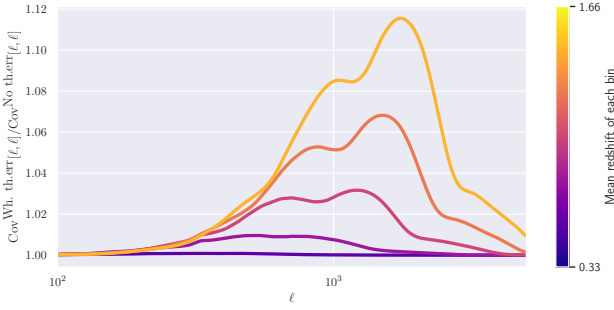


Figure 6. Ratio of the diagonals of auto-spectra elements of our C_ℓ covariance matrix with our additional theoretical error to that without theoretical error. Here, we see that the amplitude of the additional theoretical error strongly depends on the redshift bins of the auto-spectra considered, with higher redshift bins containing more theoretical error than closer bins. We note that there is significant support on the off-diagonals for our theoretical covariance, and thus the total covariance with theoretical error is much larger than just the ratios showed here.

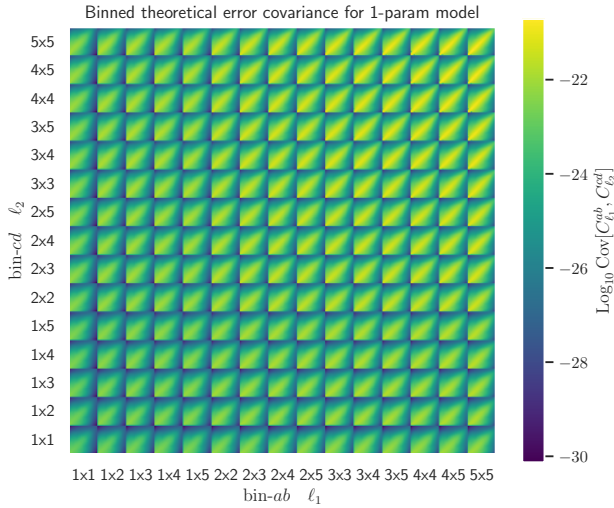


Figure 7. Plot of the binned theoretical error matrix C^E for the one-parameter model across all fifteen redshift bin combinations and twenty five binned band-powers. Here, we see that the amplitude of our theoretical error matrix generally grows as we consider higher redshift bins (e.g. the 5×5 sub-block is significantly brighter, and thus of larger magnitude, than the 1×1 sub-block). We also see that for each sub-block, the theoretical error is greatest along the $\ell_1 = \ell_2$ diagonal, though there is significant support along the off-diagonal terms, which serves to increase the overall effect of our theoretical uncertainty modelling.

4.4.3 One-parameter model

In general, the one-parameter model without additional theoretical error produces a significant biases in the recovered parameters, with at least a 3σ offset in either Ω_m or S_8 for all hydro-sims excluding BAHAMAS (recall that the one-parameter model was constructed by fitting to BAHAMAS data only). The results of the very significant biases in the remaining five hydro-sims shows that the one-parameter model of baryon feedback for a *Euclid*-like survey up to $\ell_{\max} = 5000$ is completely impractical if we wish to recover unbiased results from the analyses of cosmic shear data.

When we introduce our additional theoretical error into the analysis, we see that biases in both cosmological parameters fall dramatically across all hydro-sims for our one-parameter model. We see a

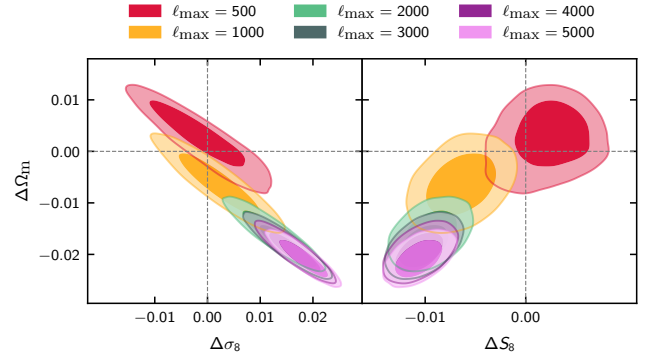


Figure 8. 2D Ω_m - σ_8 and Ω_m - S_8 offset contours for the one-parameter baryon feedback model for the SIMBA hydro-sim for a range of maximum ℓ -modes considered in the analysis. As we increase ℓ_{\max} , we are increasing the number of modes that are contaminated by baryon feedback, and thus bias our cosmological parameters away from the fiducial value. It is interesting to note that that even for the $\ell_{\max} = 1000$ analysis, which is a considerably conservative scale-cut even for Stage-III surveys (e.g. HSC-Y3, Dalal et al. 2023), our results are biased by more than 2σ in all cosmological parameters for our Stage-IV-like survey when using SIMBA as the ground-truth.

reduction in both the raw offset values, and a significant decrease in the relative bias in terms of each parameter's standard deviation. This demonstrates our theoretical uncertainties modelling is correctly identifying the scales in which baryonic feedback are not correctly modelled by the one-parameter model, down-weighting them in our analyses, and thus resulting in significantly less biased cosmological parameter constraints. However, we still see significant ($> 1\sigma$) biases in many hydro-sims even when using theoretical error. This is due to the one-parameter model being inadequate when considering a *Euclid*-like weak lensing survey.

4.4.4 Three- and six-parameter models

As expected, the more general three- and six-parameter models result in smaller absolute biases, which reflects their ability to better match more general baryon feedback scenarios, but at the cost of decreased precision due to the need to marginalise over more parameters. Hence, we see that the relative biases show a strong decrease when going to our many-parameter versions, which is an effect of decreased absolute bias and increased uncertainties.

Figure 9 plots the 2D Ω_m - σ_8 and Ω_m - S_8 offset contours for our three baryon feedback models with and without our theoretical error added for the Simba hydro-sim. This highlights the degeneracies that exist between these parameters, finding the usual ‘lensing banana’ that is the natural degeneracy between Ω_m and σ_8 . These contours gradually move to the origin as we increase the number of parameters in the baryon feedback model, and increase in size as we are marginalising over more parameters.

Figure 10 plots the 2D Ω_m - σ_8 offset contours for the one-parameter model for our suite of hydro-sims for the case of with and without our theoretical error. We see that without the theoretical error the recovered contours are highly constraining, which is a result of marginalising over a single baryon feedback parameter only, with a large degree of scatter between the hydro-sims. It is interesting to note that this scatter appears to be roughly along the degeneracy direction, though it appears random which quadrant each hydro-sim falls into.

Table 3. Table summarising our results for the bias in Ω_m as found from our MCMC analyses using our suite of six hydro-sims and three baryon feedback models, without and with our additional theoretical error modelling added to the covariance matrix when going to $\ell_{\max} = 5000$. We see that without theoretical error, the one-parameter model generally produces significant biases ($> 3\sigma$) from the true value, with only BAHAMAS giving small biases in Ω_m and S_8 . These biases reduce to less than 1σ with the inclusion of our theoretical error in the one-parameter model, highlighting the effectiveness of our theoretical error modelling. We see that the three- and six-parameter result in less bias in Ω_m , though some hydro-sims still give large biases for the six-parameter model (i.e. SIMBA and EAGLE). The inclusion of our theoretical error covariance into the three- and six-parameter models further reduces the bias.

Hydro-sim and model	$100\Delta\Omega_m$ No th. err.	$\Delta\Omega_m/\sigma_{\Omega_m}$ No th. err.	$100\Delta\Omega_m$ With th. err.	$\Delta\Omega_m/\sigma_{\Omega_m}$ With th. err.
BAHAMAS 1-param	0.057	0.258	0.038	0.098
BAHAMAS 3-param	0.012	0.038	0.049	0.127
BAHAMAS 6-param	0.100	0.276	-0.085	-0.206
EAGLE 1-param	-0.306	-1.535	0.224	0.587
EAGLE 3-param	0.149	0.520	0.433	1.186
EAGLE 6-param	0.274	0.962	0.573	1.459
HORIZON-AGN 1-param	-0.057	-0.255	0.079	0.199
HORIZON-AGN 3-param	0.224	0.631	0.123	0.331
HORIZON-AGN 6-param	0.109	0.325	0.105	0.269
ILLUSTRIS 1-param	-1.317	-5.690	0.128	0.249
ILLUSTRIS 3-param	0.048	0.127	0.373	0.828
ILLUSTRIS 6-param	0.328	0.761	0.295	0.652
SIMBA 1-param	-2.071	-8.828	-0.158	-0.293
SIMBA 3-param	-1.513	-4.723	-0.155	-0.276
SIMBA 6-param	-0.858	-2.206	-0.257	-0.567
ILLUSTRIS-TNG 1-param	-0.613	-2.885	-0.107	-0.277
ILLUSTRIS-TNG 3-param	-0.110	-0.424	0.035	0.091
ILLUSTRIS-TNG 6-param	-0.055	-0.185	0.181	0.453

Table 4. Table similar to Table 3 but now for the bias in S_8 as found from our MCMC analyses. We see that without theoretical error, the one-parameter model results in at least a 3σ bias from the true value for all hydro-sims except BAHAMAS, which reduces when going to a multi-parameter model. Our theoretical error is able to significantly reduce the bias in the one-parameter model, though we see a multi-parameter model is essential to ensure unbiased constraints across all hydro-sims.

Hydro-sim and model	$100\Delta S_8$ No th. err.	$\Delta S_8/\sigma_{S_8}$ No th. err.	$100\Delta S_8$ With th. err.	$\Delta S_8/\sigma_{S_8}$ With th. err.
BAHAMAS 1-param	0.038	0.386	-0.028	-0.101
BAHAMAS 3-param	0.083	0.492	-0.210	-0.819
BAHAMAS 6-param	0.010	0.042	-0.360	-1.468
EAGLE 1-param	0.709	8.802	0.660	2.579
EAGLE 3-param	0.240	3.742	0.360	2.039
EAGLE 6-param	0.240	3.207	0.441	2.443
HORIZON-AGN 1-param	0.574	6.002	0.464	1.616
HORIZON-AGN 3-param	0.137	0.865	0.158	0.759
HORIZON-AGN 6-param	0.165	1.070	0.089	0.448
ILLUSTRIS 1-param	0.796	3.710	0.377	1.024
ILLUSTRIS 3-param	0.208	0.950	0.253	0.867
ILLUSTRIS 6-param	0.325	1.289	0.135	0.435
SIMBA 1-param	-1.059	-7.096	0.081	0.207
SIMBA 3-param	-1.235	-6.469	-0.180	-0.480
SIMBA 6-param	-0.916	-4.903	-0.328	-1.156
ILLUSTRIS-TNG 1-param	0.281	3.701	0.033	0.130
ILLUSTRIS-TNG 3-param	-0.100	-1.602	-0.193	-1.083
ILLUSTRIS-TNG 6-param	-0.106	-1.628	-0.122	-0.715

4.4.5 Dependency on σ_k and σ_z

In our propagated covariance matrix (Equation 11) we introduced two coupling scales, σ_k and σ_z , which were both set at 0.25 in our fiducial analyses. Here, we investigate the effects of changing their values, and the effects it has on parameter constraints. We note that

in our fiducial analyses, the baryon feedback physics of the SIMBA simulation is strong enough that even the six-parameter model of baryon feedback produces significantly biased cosmological parameter constraints (Figure 12). Thus, SIMBA is a good testing ground to see how the contours react to the changing of these values.

In general, as σ_k and σ_z increase we are increasing the number of

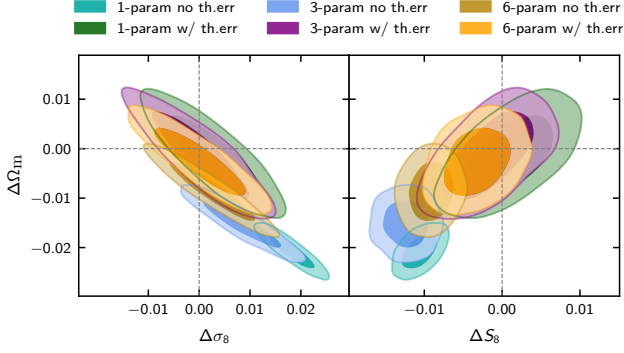


Figure 9. 2D Ω_m - σ_8 and Ω_m - S_8 offset contours for the three baryon feedback models with and without our theoretical error for the SIMBA hydro-sim. We can clearly see that the one-parameter model without theoretical error (light grey contour) produces a tight constraint on our cosmological parameters that is extremely far from the correct value. When we add our theoretical error to the data covariance (dark green contour), we find that the one-parameter model is able to recover the correct values, with an appropriate increase in the size of the contour. We see that the three- and six-parameter models, while more flexible, are unable to correctly recover unbiased results without the addition of our theoretical uncertainties.

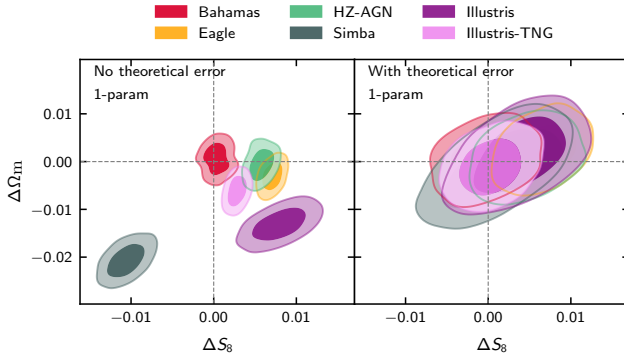


Figure 10. 2D Ω_m - S_8 offset contours for the one-parameter baryon feedback model without and with the addition of our theoretical error for our range of hydro-sims considered. We can see that without theoretical error, the one-parameter model produces a large degree of scatter for all hydro-sims, with only BAHAMAS being consistent with the input cosmology. With the introduction of theoretical error, we see that the contours increase and all except EAGLE become unbiased at the 2σ level.

wavenumber and redshift modes that contribute to a given (ℓ_1, ℓ_2) pair, respectively. This increases the size of our ℓ -space theoretical error covariance, further suppressing the high- ℓ modes that are contaminated by baryonic feedback. However, in the limit that σ_k and σ_z tend to infinity, then both Gaussian terms tend to unity and the double integral becomes factorisable in (k, k') -space and thus is equivalent to some rank-1 update of the form $\mathbf{x}\mathbf{x}^T$, where \mathbf{x} is some vector in ℓ -space. Since this is a rank-1 addition to our data covariance matrix, this is equivalent to marginalisation over a single parameter. However, since we know that single parameter models for baryonic feedback do not correctly model the wide range of behaviour of baryonic feedback effects seen in the hydro-sims, it would be incorrect to take this limit for the values of σ_k and σ_z .

The regime in which our theoretical error covariance reduces to a rank-1 matrix will be determined by the maximum k -space difference between different ℓ -modes. For example, Figure 2 shows that there is an approximate two decade difference in $\log k$ between our smallest

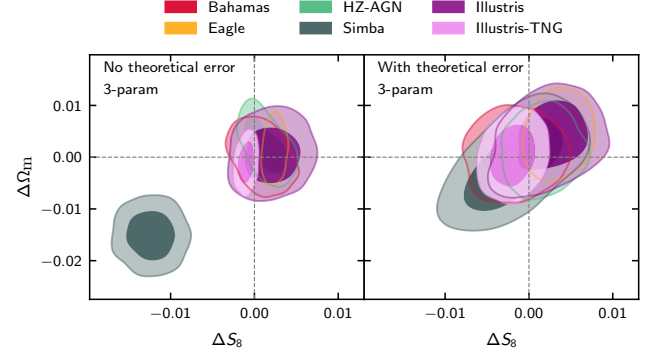


Figure 11. 2D Ω_m - S_8 offset contours for the three-parameter baryon feedback model without and with the addition of our theoretical error for our range of hydro-sims considered. When compared to the less flexible one-parameter model, we see that the three parameter model without additional theoretical error is better able to recover the input cosmology for a wider range of simulations, though EAGLE, ILLUSTRIS-TNG, and SIMBA remain biased to at least the 2σ level. We note the general increase in the contour's area going from the one- to three-parameter model which is associated with marginalising over more baryon feedback parameters. We see that with theoretical error, all contours are unbiased at the 2σ level.

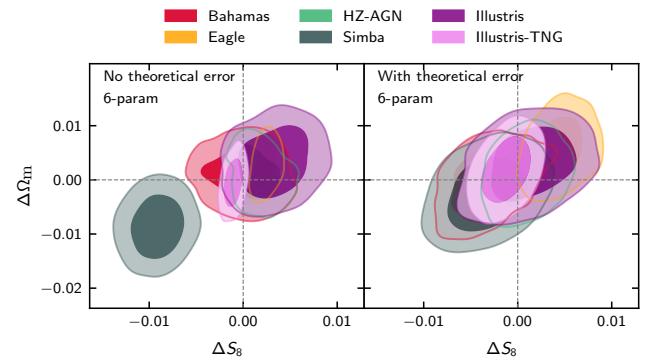


Figure 12. 2D Ω_m - S_8 offset contours for the one-parameter baryon feedback model without and with the addition of our theoretical error for our range of hydro-sims considered. Again, we see an extension of the general trend in the contours without additional theoretical error: an increase in the contours with them moving towards the origin. We see that even with a six-parameter model, it is not sufficient to recover unbiased constraints from the SIMBA simulation.

and largest ℓ -mode. Thus, if one were to choose a value for σ_k that easily encompassed these values within one standard deviation, then we would expect our theoretical error covariance to collapse to the rank-1 limit. Since our values chosen for σ_k are much less than two decades, we expect that our values to not fall within this limit.

In Figure 13, we plot the 2D contours for three different combinations of σ_k and σ_z . Larger values of these parameters allows for longer-scale correlations in wavenumber and redshift, and thus produce a larger amplitude for the theoretical error covariance matrix. Figure 13 shows that these larger values suppress high- ℓ modes more than for smaller values, which is seen by the larger contours and a reduction in the bias from baryon feedback. While on the range of values that we tested larger values increase the effectiveness of the theoretical error covariance, larger values also increase the correlation length between different wavenumbers and redshifts in the covariance matrix which decreases the adaptability of our theoretical error covariance to match more general models of baryon feedback

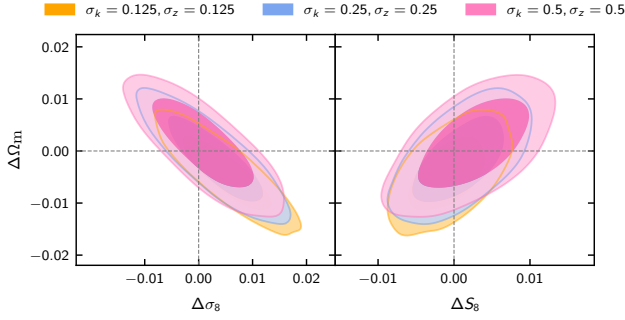


Figure 13. 2D Ω_m - σ_8 and Ω_m - S_8 contours for the Simba hydro-sim using the one-parameter model with theoretical error where we are changing the values of σ_k and σ_z . Here, we see that as we increase their values, the effects of the theoretical error covariance become larger - increasing the size and decreasing the biases in the contours.

physics. In the limit that these values go to infinity, we would be saying that all wavenumbers and redshifts are 100 % correlated, which is unphysical since we know that baryonic effects in the power spectrum are quite local at high k . Equally, in the limit that these values go to zero, we would be maximally destroying information through the covariance matrix by assuming that each wavenumber and redshift has an independent error which are uncorrelated between similar modes. Ultimately, there is less than a 1σ shift in contours plotted in Figure 13, and so our implementation of the theoretical error approach is broadly insensitive to the values of σ_k and σ_z .

We investigate the effects of changing these coupling parameters in our three- and six-parameter models in Appendix A, which shows a similar trend to the one-parameter model in that larger values produce increased contours with less baryonic bias in them.

4.4.6 Growth-structure split

The information in the cosmic shear power spectrum (Equation 4) comes from two pieces: the geometrical factors of the lensing kernels, and in the matter power spectrum, both depending on the matter density Ω_m . It can be advantageous to decouple this matter density in two: a factor that describes the geometry of the Universe through the computation of the comoving distances in the lensing kernel, $\Omega_{m, \text{geom}}$, and the growth of structure in the universe that is used in the computation of the matter power spectrum, Ω_m (Matilla et al. 2017). This growth-structure split of the matter density has been applied to existing cosmic shear data-sets, including the Dark Energy Survey (Muir et al. 2021; Zhong et al. 2023) and the Kilo-Degree Survey (Ruiz-Zapatero et al. 2021).

We are motivated to apply this growth-structure split to our approach of modelling the theoretical uncertainties at the matter power spectrum level. By quantifying the errors directly in $P(k)$, and then propagating to the angular power spectrum, we are hopefully preserving information in the lensing kernels. Our lensing kernels have no theoretical uncertainties associated with them, and so we hope to preserve information about $\Omega_{m, \text{geom}}$ even with our scale cuts present.

Thus, we can repeat a sub-set of our MCMC analyses to investigate how the inclusion of our theoretical error changes the constraints on Ω_m and $\Omega_{m, \text{geom}}$. This is presented in Figure 14. Here, we see that without our theoretical uncertainties, the inflexible one-parameter model leads to a bias in Ω_m but remains unbiased in the geometrical term $\Omega_{m, \text{geom}}$. This tells us that while our data-vector may still be contaminated with baryonic feedback from the matter power spectrum, information from the lensing kernels can still be extracted from cos-

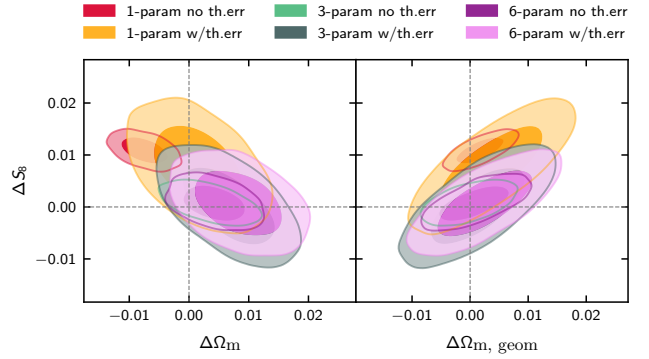


Figure 14. 2D Ω_m - S_8 and $\Omega_{m, \text{geom}}$ - S_8 contours for different baryon feedback models without and with the addition of our theoretical error with the EAGLE hydro-sim. We see that without theoretical error, the one-parameter model produces results that are biased in S_8 and Ω_m , but can identify that the information from the lensing kernels is not affected by baryonic feedback, and thus produces unbiased estimates for $\Omega_{m, \text{geom}}$.

mic shear data. When we introduce our theoretical error terms to the covariance matrix, we down-weight baryonic contaminated modes, and so become consistent in Ω_m and $\Omega_{m, \text{geom}}$ at the cost of increased contour sizes.

5 DISCUSSION AND CONCLUSIONS

We have presented results for parameter constraints using various hydrodynamical simulations as ground truths analysed with three different baryon feedback models, with and without an additional theoretical error covariance. We have seen that constraints on cosmological parameters are significantly biased for a forthcoming Stage-IV like cosmic shear survey using as low as a maximum ℓ -mode of $\ell_{\text{max}} = 1000$ when analysing the hydrodynamical simulation's data using a single parameter for baryon feedback. This is consistent with previous results in the literature, for example Doux et al. (2021) finding a harmonic-space scale cut of $\ell_{\text{max}} \sim 500$ was needed for the case of DES-Y3 mock data against a model without baryonic feedback in.

Hence, we are motivated to more accurately model the errors associated in the matter power spectrum arising from baryon feedback over the more traditional binary scale-cuts approach, resulting in our theoretical error covariance. This theoretical error was then applied to our model of baryon feedback across our suite of hydrodynamical simulations, finding that our parameters biases decreased with smaller absolute and relative off-sets when going to the same maximum multipole in our analysis.

We note that some hydro-sims still yield a significant ($>1\sigma$) bias in cosmological parameters when using our theoretical error covariance for the single-parameter model, which indicates that such a basic model will be unsuitable for application to Stage-IV cosmic shear survey data. While the multi-parameter models tended to do better in producing unbiased results, our theoretical error covariance was still needed to ensure that all hydro-sim results were unbiased when going to $\ell_{\text{max}} = 5000$.

The theoretical error formalism is a general method for quantifying the known errors of a method to realisations of the data. This method can be applied to a wide-range of modelling problems within cosmology and astrophysics, where we have applied it to baryonic feedback within the matter power spectrum. To that end, the theoretical error is not a fixed quantity. If next generation hydrodynamical simulations release that feature, for example, improved subgrid models of

physical processes that we know we are currently lacking (Crain & van de Voort 2023), then it would make sense to replace the older simulations in our suite with these new releases. This would alter our error envelope function, improving or reducing our degree of trust in our numerical baryonic feedback models. Alternatively, as new baryonic feedback models are developed which are more accurate to the hydro-sims, the need for a theoretical error covariance becomes diminished.

With multi-parameter models of baryonic feedback, the effectiveness of external priors (that is, information on baryonic feedback not from cosmic shear alone) become increasingly powerful. In recent years, observational constraints on baryonic feedback have come from the thermal Sunyaev-Zeldovich effect in CMB observations (Tröster et al. 2022), and diffuse x-ray backgrounds (Ferreira et al. 2024). With ever increasing precision data taken on our Universe across the entire electromagnetic spectrum, the power of external priors and cross-correlation with Stage-IV cosmic shear surveys for baryonic feedback physics constraints will be immense.

The Holy Grail of baryonic feedback models will, of course, be a model that can fit all hydro-sims with no free parameters.⁴ However, while we are making progress towards this goal, for example BACCO (Aricò et al. 2021), a theoretical error covariance is highly valuable until then. We expect the formalism that we have presented and validated here will be of significant value to forthcoming Stage-IV weak lensing surveys.

ACKNOWLEDGEMENTS

We acknowledge HPC resources from the IRIS computing consortium. AH acknowledges support from a Royal Society University Research Fellowship. For the purpose of open access, the author has applied a Creative Commons Attribution (CC BY) licence to any Author Accepted Manuscript version arising from this submission.

REFERENCES

Abate A., et al., 2012, arXiv e-prints (1211.0310)
 Abbott T. M. C., et al., 2022, *Phys. Rev. D*, 105, 023520
 Abbott T. M. C., et al., 2023, *Open J. Astrophys.*, 6, 2305.17173
 Amon A., et al., 2022, *Phys. Rev. D*, 105, 023514
 Aricò G., Angulo R. E., Contreras S., Ondaro-Mallea L., Pellejero-Ibañez M., Zennaro M., 2021, *Mon. Not. Roy. Astron. Soc.*, 506, 4070
 Asgari M., et al., 2021, *Astron. Astrophys.*, 645, A104
 Baldauf T., Mirbabayi M., Simonović M., Zaldarriaga M., 2016, arXiv e-prints 1602.00674
 Bartelmann M., 2010, *Class. Quant. Grav.*, 27, 233001
 Bartelmann M., Schneider P., 2001, *Phys. Rept.*, 340, 291
 Blanchard A., et al., 2020, *Astron. Astrophys.*, 642, A191
 Chisari N. E., et al., 2018, *Mon. Not. Roy. Astron. Soc.*, 480, 3962
 Chisari N. E., et al., 2019, *Open J. Astrophys.*, 2, 4
 Chudaykin A., Ivanov M. M., 2019, *JCAP*, 11, 034
 Cooray A., Sheth R. K., 2002, *Phys. Rept.*, 372, 1
 Copeland D., Taylor A., Hall A., 2018, *Mon. Not. Roy. Astron. Soc.*, 480, 2247
 Crain R. A., van de Voort F., 2023, *Ann. Rev. Astron. Astrophys.*, 61, 473
 Dalal R., et al., 2023, *Phys. Rev. D*, 108, 123519

Davé R., Anglés-Alcázar D., Narayanan D., Li Q., Rafieferantsoa M. H., Appleby S., 2019, *Mon. Not. Roy. Astron. Soc.*, 486, 2827
 Doux C., et al., 2021, *Mon. Not. Roy. Astron. Soc.*, 503, 3796
 Doux C., et al., 2022, *Mon. Not. Roy. Astron. Soc.*, 515, 1942
 Elbers W., et al., 2024, arXiv e-prints 2403.12967
 Ferreira T., Alonso D., Garcia-Garcia C., Chisari N. E., 2024, *Phys. Rev. Lett.*, 133, 051001
 Giri S. K., Schneider A., 2021, *JCAP*, 12, 046
 Hall A., Taylor A., 2022, *Phys. Rev. D*, 105, 123527
 Handley W. J., Hobson M. P., Lasenby A. N., 2015a, *Mon. Not. Roy. Astron. Soc.*, 450, L61
 Handley W. J., Hobson M. P., Lasenby A. N., 2015b, *Mon. Not. Roy. Astron. Soc.*, 453, 4385
 Heymans C., et al., 2021, *Astron. Astrophys.*, 646, A140
 Huang H.-J., Eifler T., Mandelbaum R., Dodelson S., 2019, *Mon. Not. Roy. Astron. Soc.*, 488, 1652
 Kilbinger M., 2015, *Rept. Prog. Phys.*, 78, 086901
 Kitching T. D., Taylor A. N., 2011, *Mon. Not. Roy. Astron. Soc.*, 416, 1717
 Krause E., et al., 2021, arXiv e-prints 2105.13548
 Laureijs R., et al., 2011, arXiv e-prints (1110.3193)
 Li X., et al., 2023a, *Phys. Rev. D*, 108, 123518
 Li S.-S., et al., 2023b, *Astron. Astrophys.*, 679, A133
 Matilla J. M. Z., Haiman Z., Petri A., Namikawa T., 2017, *Phys. Rev. D*, 96, 023513
 McCarthy I. G., Schaye J., Bird S., Le Brun A. M. C., 2017, *Mon. Not. Roy. Astron. Soc.*, 465, 2936
 Mead A., Peacock J., Heymans C., Joudaki S., Heavens A., 2015, *Mon. Not. Roy. Astron. Soc.*, 454, 1958
 Mead A., Heymans C., Lombriser L., Peacock J., Steele O., Winther H., 2016, *Mon. Not. Roy. Astron. Soc.*, 459, 1468
 Mead A., Brieden S., Tröster T., Heymans C., 2020, *Mon. Not. Roy. Astron. Soc.*, 502, 1401
 Mellier Y., et al., 2024, arXiv e-prints (2405.13491)
 Mohammed I., Seljak U., 2014, *Mon. Not. Roy. Astron. Soc.*, 445, 3382
 Moreira M. G., Andrade-Oliveira F., Fang X., Huang H.-J., Krause E., Miranda V., Rosenfeld R., Simonović M., 2021, *Mon. Not. Roy. Astron. Soc.*, 507, 5592
 Muir J., et al., 2021, *Phys. Rev. D*, 103, 023528
 Nelson D., et al., 2015, *Astron. Comput.*, 13, 12
 Ni Y., et al., 2023, *Astrophys. J.*, 959, 136
 Peacock J. A., Smith R. E., 2000, *MNRAS*, 318, 1144
 Pellejero-Ibanez M., Angulo R. E., Zennaro M., Stuecker J., Contreras S., Arico G., Maion F., 2023, *Mon. Not. Roy. Astron. Soc.*, 520, 3725
 Ruiz-Zapatero J., et al., 2021, *Astron. Astrophys.*, 655, A11
 Salcido J., McCarthy I. G., 2024, arXiv e-prints 2409.05716
 Salcido J., McCarthy I. G., Kwan J., Upadhye A., Font A. S., 2023, *Mon. Not. Roy. Astron. Soc.*, 523, 2247
 Schaye J., et al., 2015, *Mon. Not. Roy. Astron. Soc.*, 446, 521
 Schneider A., Teyssier R., 2015, *JCAP*, 12, 049
 Schneider A., et al., 2016, *JCAP*, 04, 047
 Schneider A., Teyssier R., Stadel J., Chisari N. E., Le Brun A. M. C., Amara A., Refregier A., 2019, *JCAP*, 03, 020
 Secco L. F., et al., 2022, *Phys. Rev. D*, 105, 023515
 Seljak U., 2000, *Mon. Not. Roy. Astron. Soc.*, 318, 203
 Semboloni E., Hoekstra H., Schaye J., van Daalen M. P., McCarthy I. J., 2011, *Mon. Not. Roy. Astron. Soc.*, 417, 2020
 Smith R. E., et al., 2003, *Mon. Not. Roy. Astron. Soc.*, 341, 1311
 Spergel D., et al., 2015, arXiv e-prints (1503.03757)
 Sprenger T., Archidiacono M., Brinckmann T., Clesse S., Lesgourgues J., 2019, *JCAP*, 02, 047
 Springel V., et al., 2018, *Mon. Not. Roy. Astron. Soc.*, 475, 676
 Takahashi R., Sato M., Nishimichi T., Taruya A., Oguri M., 2012, *Astrophys. J.*, 761, 152
 Tröster T., et al., 2022, *Astron. Astrophys.*, 660, A27
 Upham R. E., Brown M. L., Whittaker L., 2021, *Mon. Not. Roy. Astron. Soc.*, 503, 1999
 Vogelsberger M., Marinacci F., Torrey P., Puchwein E., 2020, *Nature Rev. Phys.*, 2, 42

⁴ This is not a requirement on the baryonic feedback models, per se, but on the requirements on the ensemble of hydrodynamical simulations to converge to a single prediction for the evolution of $P^{\text{Hy}}(k, z)$. With no scatter in the hydro-sims, deriving a fitting formulae for baryonic feedback physics becomes trivial.

- Zhong K., Saraivanov E., Miranda V., Xu J., Eifler T., Krause E., 2023, *Phys. Rev. D*, 107, 123529
- Zuntz J., et al., 2015, *Astron. Comput.*, 12, 45
- van Daalen M. P., Schaye J., Booth C. M., Vecchia C. D., 2011, *Mon. Not. Roy. Astron. Soc.*, 415, 3649
- van Daalen M. P., McCarthy I. G., Schaye J., 2020, *Mon. Not. Roy. Astron. Soc.*, 491, 2424

APPENDIX A: DEPENDENCY OF THE COVARIANCE ON THE COUPLING PARAMETERS

In Section 4.4.5 we looked at the one-parameter model and its dependency on the coupling parameters σ_k and σ_z . Here, we present a comparison between all three baryon feedback models and investigate their dependency on the coupling parameters. Figure A1 uses SIMBA as the ground-truth, which features quite significant baryonic feedback, and Figure A2 using ILLUSTRIS-TNG, which has less extreme feedback. When using SIMBA as the ground-truth, we see a that there is a strong link between the coupling parameter’s values and the cosmological parameter biases for the one-parameter model, whereas the more general three- and six-parameter models are approximately insensitive to σ_k and σ_z due to their ability to better fit the data (thus have less significant theoretical uncertainties associated with these models). We also see that, when using ILLUSTRIS-TNG as the ground-truth, since all three feedback models can adequately fit the data, increasing σ_k and σ_z serves to slightly broaden the contours only, with no significant effect on the parameter means.

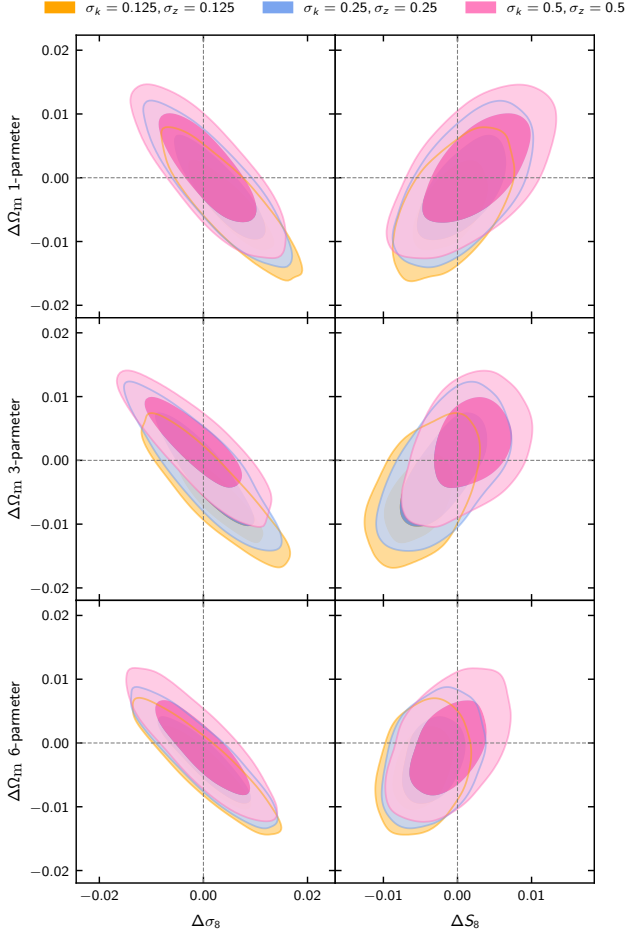


Figure A1. Ω_m - σ_8 and Ω_m - S_8 contours for the SIMBA hydro-sim using the one-, three-, and six-parameter models (descending rows) with theoretical error for different values of σ_k and σ_z (different coloured contours). We see that increasing these values produces a stronger effect for the theoretical covariance, increasing the suppression of small-scale modes and thus reducing the bias from baryonic feedback.

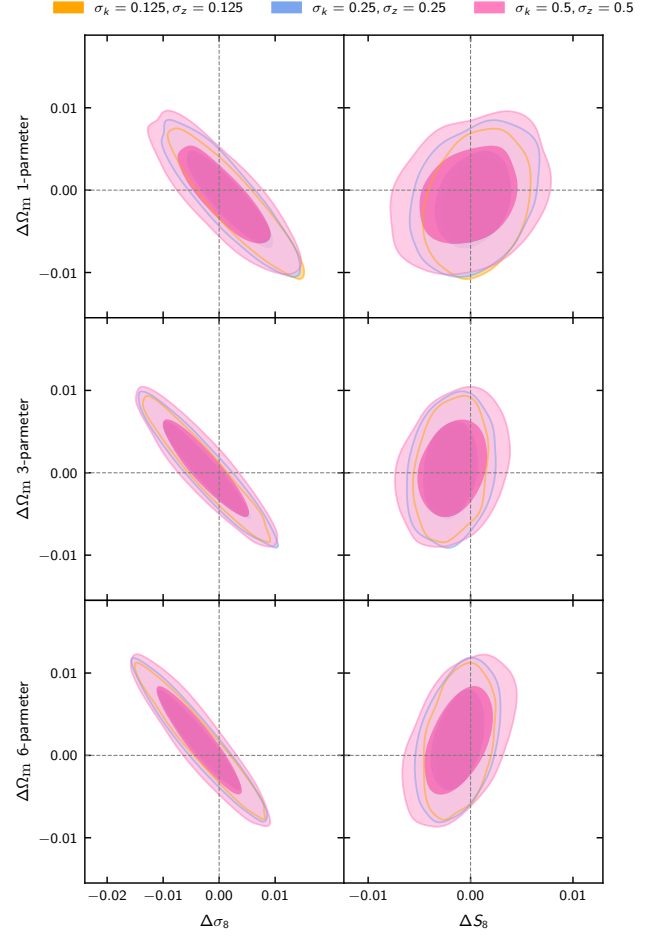


Figure A2. Similar plot to Figure A1, but for the ILLUSTRIS-TNG hydro-sim instead of SIMBA. Since ILLUSTRIS-TNG can be well fitted by each of our HMCODE models with theoretical error, the effect of changing σ_k and σ_z is just to increase or decrease the size of the contours, without effecting the bias in these parameters.

This paper has been typeset from a \LaTeX file prepared by the author.